Desalination and Water Treatment
www.deswater.com

doi: 10.5004/dwt.2021.26795

216 (2021) 358–371
March

Kinetics and equilibrium studies of methylene blue dye adsorption on oil palm frond adsorbent

Amy Low Huey Chuein[a], Nor Najhan Idris[a], Tuan Sherwyn Hamidon[a], Nur Fatin Silmi Mohd Azani[a], Nor Salmi Abdullah[b], Syazrin Shima Sharifuddin[b], Ang Shin Ying[b], M. Hazwan Hussin[a,*]

[a]*Materials Technology Research Group (MaTReC), School of Chemical Sciences, Universiti Sains Malaysia, 11800 Minden, Penang, Malaysia, Tel. +60 4 653 6378; Fax: +60 4 657 4854; emails: mhh@usm.my/mhh.usm@gmail.com (M.H. Hussin), amylow95@yahoo.com (A.L.H. Chuein), najhan_idris@yahoo.com (N.N. Idris), tuansherwyn.hamidon@gmail.com (T.S. Hamidon), fatinsilmi2@gmail.com (N.F.S.M. Azani)*
[b]*National Hydraulic Research Institute of Malaysia (NAHRIM), Jalan Putra Permai, Seri Kembangan, Selangor Darul Ehsan, Malaysia, Tel. +603 8947 6400; emails: norsalmi@nahrim.gov.my (N.S. Abdullah), syima@nahrim.gov.my (S.S. Sharifuddin), syang@nahrim.gov.my (A.S. Ying)*

Received 16 February 2020; Accepted 8 November 2020

ABSTRACT

Oil palm fronds (OPF) with a moisture content of 1.1% were used to prepare oil palm frond adsorbent (OPFAD) using chemical activation method, which consisted of impregnation treatment of OPF (10–15 mm) with potassium hydroxide at a ratio of 1:1, followed by carbonization at 400°C by N_2 under a steady flow rate of 1 mL min^{-1} for 3 h. Batch adsorption studies were conducted to investigate the adsorptive properties of oil palm frond adsorbent towards the removal of methylene blue dye. In this research, OPFAD was classified as mesopores with reference from the International Union of Pure and Applied Chemistry with 2.7273 m^2 g^{-1} of Brunauer–Emmett–Teller surface area, 0.003112 cm^3 g^{-1} of total pore volume, and 4.56361 nm of average pore diameter. The maximum removal percentage of methylene blue through the employment of OPFAD was 82.8% obtained at an adsorbent dosage of 0.1 g/100 mL and an initial dye concentration of 40 ppm. The experimental data from the adsorption process were fitted well into the pseudo-second-order kinetic model and Langmuir isotherm with a Gibbs free energy of adsorption ($\Delta G°$) of –24.36 kJ mol^{-1}. Based on the present research study, it can be proposed that OPFAD can act as an effective alternative adsorbent.

Keywords: Oil palm fronds; Adsorption; Chemical activation; Methylene blue

1. Introduction

Dyes-bearing sewage discharged by textile, paint, paper, plastic, and leather industries have become a significant concern. It was reported that more than 700,000 metric tons of commercial dyes were produced annually with over 5%–10% discharged into industrial wastewaters [1,2]. Methylene blue (MB) is a cationic dye having significant applications in dyeing industries. However, MB imparts adverse effects to humans such as increased heart rate, vomiting, shock, cyanosis, jaundice, and necrosis [3]. Thus, it is essential to remove MB dye from the process effluent.

Several efforts in wastewater treatment processes include adsorption, biosorption, coagulation/flocculation, advanced oxidation, ozonation, membrane filtration, ultrafiltration, photochemical degradation, and liquid–liquid

* Corresponding author.

extraction [2,4]. Among all adsorption had notably surpassed the others because of its high efficiency and economic feasibility [2,4,5]. In recent years, activated carbon derived from various biowastes and wood biomass, such as mangosteen peel waste [6], banana trunk waste [7], and *Acacia mangium* wood [8] have been studied for the adsorption of dyes. Activated carbon is a common and efficient adsorbent used to remove dyes from wastewaters because of its large surface area, high adsorption capacity, and diverse functional groups [9]. However, commercial activated carbon (CAC) remains limited due to the high cost resulting from the use of non-renewable and expensive starting materials, such as coal [4]. Therefore, there are great interests in finding inexpensive, renewable, and effective agricultural waste-based alternatives to replace the existing CAC. Low-cost agricultural waste materials that have been successfully used to manufacture activated carbon in the recent past include waste tea [1], apricot stones [4], coconut shell [10], and oil palm biomass [3,11].

In Malaysia, the palm oil industry is one of the critical agro-industries which generate a massive amount of oil palm wastes in the form of leaves, trunks, fronds, empty fruit bunches, fibers, and shells [12]. It was reported that in 2010, nearly 80 million tons of oil palm waste was generated by the industry and is estimated to increase up to 100 million tons by the year 2020 [3]. Despite no economic value, these wastes have created a severe disposal problem. Therefore, made use of the oil palm wastes as an alternative low-cost adsorbent would be beneficial from both environmental and economic points of view.

In this study, oil palm fronds (OPF) were chosen as a low-cost precursor for the production of an efficient adsorbent for the adsorption of MB owing to its effective adsorption performance in pesticides and herbicides [13,14]. In a previous study, oil palm empty fruit bunches (OPEFB) have been used for methyl orange (MO) dye adsorption [15]. To the best of our knowledge, no comprehensive study has been reported on the adsorption of MB by oil palm frond adsorbent (OPFAD). Therefore, the objectives of this study are to prepare a low-cost adsorbent from oil palm fronds (OPFAD) through chemical activation and to characterize through Fourier transform infrared spectroscopy (FTIR), thermogravimetric analysis (TGA), Brunauer–Emmett–Teller (BET), scanning electron microscopy (SEM), energy-dispersive X-ray spectroscopy (EDX), and CHN analyses. The ability of OPFAD as a potential adsorbent to remove MB dye was studied via a batch adsorption system. The effect of adsorbent dosage, pH in the dye, as well as initial concentration and contact time of MB adsorption were studied. Adsorption isotherms and kinetics were investigated to evaluate experimental data.

2. Experimental

2.1. Materials

OPF were collected from oil palm plantation at Tikam Batu, Sungai Petani, Kedah in September 2018. All the chemicals used were analytical reagent grade (QRëC), including hydrochloric acid 37%, sulfuric acid 97%, and methylene blue powder. CAC was procured from QRec (ASIA) Sdn Bhd. Distilled water provided in the lab was used in all experiments. The OPF leaves were removed, and the strands were chopped into small pieces. Upon sun drying for 2 d, the chips were then ground to a 1–3 mm particle size using a Wiley mill, and the fiber was further dried in an oven at 50°C for 24 h. Milled dried OPF was kept in an airtight container for further use. Proximate analysis was carried out to determine the composition (% w/w) of milled, dried OPF. It was found to contain 0.97% ± 0.21% moisture content, 3.00% ± 0.20% ash content, 8.5% ± 1.47% extractives content, 37.65% ± 1.46% cellulose content, 31.64% ± 0.71% hemicellulose content and 18.37% ± 1.47% Klason lignin.

2.2. Preparation of OPFAD

The acquired OPF was used as a precursor. The thorns and leaflets of OPF were removed using a knife and a scissor. Then, the OPF was cut into small dice-like shape using a blade and knife. The chipped OPF was repeatedly washed to remove any solid impurities and sundried. Then, it was stored in an oven at 105°C overnight. The preparation of the adsorbent from OPF was prepared following the method as reported by Njoku et al. [16] with slight modifications, where Njoku et al. [16] soaked coconut fronds in orthophosphoric acid (H_3PO_4) instead of 10% KOH used in the present study. The chipped dried OPF then underwent chemical impregnation. About 20 g of chipped dried OPF was mixed with 200 mL freshly prepared 10% KOH in 1:1 ratio by weight. The mixture was stirred using a magnetic stirrer for 24 h to ensure full absorption of reagent into raw materials. The temperature of the stirring process was kept at 70°C to evaporate the excess water. Then, the mixture was filtered and washed with excess distilled water until the filtrate pH reached a range of 6.0–7.0. The impregnated OPF was dried in the oven at 105°C overnight.

The impregnated OPF then underwent carbonization (first process) using a tubular electric furnace. The OPF was placed in a steel crucible and inserted into a stainless tubular electric furnace, where it underwent carbonization at 400°C under a steady gas flow (purified nitrogen) of 1 mL min^{-1} for 3 h, in contrast to the activation process carried out by Njoku et al. [16] using a stainless steel vertical electric tubular furnace at 500°C under purified nitrogen with a flow rate of 150 mL min^{-1} for 2 h. The second process of activation was continued using N_2 gas under the same conditions and held for 2 h. OPFAD was cooled to room temperature before removing out from the furnace. OPFAD was then washed repeatedly with warm distilled water to eliminate any remaining KOH. OPFAD was, again, washed until the filtrate pH reached the range of 6.0–7.0. The washed OPFAD was dried in the oven at 105°C overnight. Finally, dried OPFAD was crushed into fine powder form using mortar and pestle. The powdered OPFAD was kept in an airtight container for further analyses.

2.3. FTIR analysis

The functional groups of CAC and OPFAD were identified by FTIR analysis (Perkin Elmer System 2000 spectrometer, USA). Both samples were prepared using the KBr method by mixing the samples with potassium bromide

with 1:100 weight ratio of sample to KBr. The spectra were recorded for 20 scans per sample in the transmittance mode at 4,000–400 cm^{-1} with a resolution of 4.0 cm^{-1}.

2.4. TGA analysis

TGA analysis of CAC and OPFAD were analyzed using thermogravimetric analyzer Perkin-Elmer STA 6000. The samples were heated from 30°C to 900°C at 10°C min^{-1} and held for 5 min at the highest temperature, which was 900°C before cooling it down to 30°C to proceed to the second heating.

2.5. N_2-BET analysis

Prior to nitrogen adsorption, the samples were degassed at 280°C for 8 h in a vacuum atmosphere. BET surface area, total pore volume, and average pore diameter for adsorption of CAC, OPF, and OPFAD were analysed using BET equation and Quantachrome Nova Win2© 1994–2002.

2.6. SEM/EDX analyses

The morphology of OPF and OPFAD were analyzed by SEM analysis. SEM micrographs were obtained at a magnification of 3,000× and an electron beam voltage of 10 kV. A small amount of OPF powder and OPFAD powder were dispersed to a carbon stud and the samples were placed in the QUANTA FEI 650 for SEM analysis. Meanwhile, the elemental analysis was analyzed using EDX spectroscopy (QUANTA FEI 650).

2.7. CHN analysis

The elemental composition of carbon, hydrogen, and nitrogen of CAC, OPF, and OPFAD were analyzed using a CHN analyzer. The sample was weighed in a tin capsule, and the sample amount for organic material is about 2–3 mg.

2.8. Effect of adsorbent dosage

Six different dosages of 0.01, 0.05, 0.1, 0.5, 1.0, and 5.0 g of OPFAD were used to identify the optimum dosage for removal of 100 ppm MB dye. Each of the six different flasks was filled with 25 mL of 100 ppm MB dye and different dosages accordingly. Each flask was covered using aluminum foil to protect from light penetration through the flask. The mixtures were shaken at 100 rpm for 24 h using a shaker. After 24 h, the samples were filtered, respectively, to separate OPFAD from MB dye solution. The concentrations of filtered MB solutions were analyzed using a direct reading spectrophotometer (Shimadzu, Model UV-2600).

The removal percentage (%) of 100 ppm MB solution was calculated using Eq. (1):

$$\text{Removal}\left(\%\right)=\left(\frac{C_0-C_e}{C_0}\right)\times 100 \tag{1}$$

The extent of MB solution adsorption at equilibrium, q_e (mg g^{-1}), was calculated using Eq. (2):

$$q_e=\frac{\left(C_0-C_e\right)V}{W} \tag{2}$$

where C_0 is the initial concentration of MB solution, C_e is the concentration of MB at equilibrium, V is the volume of solution in L and W is the weight of the adsorbent or optimum dosage of adsorbent in g.

2.9. Spectrophotometric determination of MB dye

The residual concentrations of methylene blue dye were measured by using UV-VIS spectrophotometer (Shimadzu UV-2600, Japan) at a wavelength of 668 nm. The standard linear calibration plot was obtained in the concentration range of 1.0–50.0 ppm, where the correlation coefficient (R^2) of the standard calibration plot for MB dye was found to be 0.9965. The limit of detection (LOD) calculated according to International Conference on Harmonization (ICH) guidelines was found to be 0.63 ppm.

2.10. Point of zero charge analysis

Point of zero charge (pH_{pzc}) analysis was determined by preparing 100 mL of distilled water with an adjusted pH of range 2–12 using 0.1 M HCl or 0.1 M NaOH. The initial pH of each adjusted solutions was recorded. Approximately 0.1 g of OPFAD was added into each adjusted pH solution and shaken at 100 rpm for 48 h. After 48 h, the mixture was filtered to separate activated carbon from adjusted pH solution. The final pH for each adjusted pH solution was recorded, and a graph of pH_{final} against $pH_{initial}$ was plotted. The intersection of line pH_{final} = $pH_{initial}$ was determined as the pH_{pzc}.

2.11. Effect of pH

The aqueous solution of MB with a pH range from 4 to 12 was prepared by adding a few drops of 0.1 M HCl or 0.1 M NaOH. The optimum dosage of 0.1 g of OPFAD was mixed with 100 mL of adjusted pH MB solutions and shaken at 100 rpm for 24 h. After 24 h, the mixture was filtered to separate activated carbons from MB solution. The concentration of the filtrate MB solution was analyzed using a direct reading spectrophotometer (UV-2600). The removal percentage of 100 ppm MB solution was calculated using Eq. (1).

2.12. Effect of contact time and kinetics studies

The adsorption equilibrium time can be studied by performing the effect of time taken by adsorbent to remove MB dye solution. The adsorption rate of adsorbent on removing MB dye solution is one of the criteria for defining the adsorbent efficiency. Approximately 0.1 g of OPFAD was mixed with 100 mL of 100 ppm MB dye solution. In order to study the effect of contact time, the mixtures were shaken at 100 rpm at a different time interval of 1, 3, 6, 12, and 24 h; while to investigate on the kinetics of adsorption, the mixtures were shaken at 100 rpm at several times range from 1 to 60 min. The concentration of MB solutions was analyzed

using a direct reading spectrophotometer (UV-2600) at 668 nm.

2.13. Effect of initial MB dye concentration

The initial MB dye solutions concentrations of 5, 20, 40, 60, 80, and 100 ppm were prepared, respectively. This is to study the rate of MB dye adsorption onto the optimum dosage of OPFAD. The optimum dosage of 0.1 g of OPFAD was added to 100 mL adjusted concentration MB solution and shaken at 100 rpm for 24 h. The MB dye solutions concentrations were monitored using direct reading spectrophotometry (UV-2600).

3. Results and discussion

3.1. FTIR analysis

FTIR spectra are used to identify the presence of the functional groups in the adsorbent, which in this study were CAC and OPFAD. Identification of the functional groups in CAC and OPFAD enhances the adsorption process where they are essential for the binding of the adsorbent. FTIR spectra of CAC and OPFAD samples are shown in Fig. 1.

The peaks in the region of 3,396–3,329 cm^{-1} correspond to the hydroxyl (–OH) groups of alcohols, phenols, carboxylic acids, and water adsorbed onto CAC and OPFAD [4,13]. The peaks at approximately 1,562–1,590 cm^{-1} for both CAC and OPFAD attributes to the C=C skeletal stretching vibration in an aromatic ring or cyclic alkene where generally found in carbonaceous material like activated carbon [4,13]. The absorption peak at 1,054 cm^{-1} can be assigned to C–O stretching vibrations in alcohols, phenols, acids, ethers, or esters [4,13,17]. The band at 1,376 cm^{-1} is characteristic of aromatic ring vibrations either with the bending vibrations of –OH bonds or with the symmetric vibration of –CH bond in methyl group [13,18]. The IR peak at 2,922 cm^{-1} is assigned to asymmetric C–H stretching [4,13].

According to the FTIR spectroscopy analysis for raw OPF reported in previous studies [19–21], the peaks in the region of 3,394–3,390 cm^{-1} correspond to the stretching of OH groups, while the peaks at 2,900–2,800 cm^{-1} are related to the C–H stretching. The peaks at 1,701–1,737 cm^{-1} in raw OPF refer to the C=O stretching of hemicellulose and lignin. It can also be noticed that the peaks at 1,509–1,609 cm^{-1} indicate the C=C aromatic skeletal vibration of lignin which only appeared in raw OPF. The sharp peaks located between 893–899 cm^{-1} are attributed to the β-glycosidic linkage of cellulose and adsorbed water in the samples.

3.2. TGA analysis

The thermal stability of CAC and OPFAD were studied by the thermogravimetric method. Derivative thermal gravimetric (DTG) and thermal gravimetric (TG) curves of CAC and OPFAD are presented in Fig. 2. DTG is used to measure the rate of weight loss, while TG is used to measure the weight loss of substances concerning the temperature of thermal degradation [22].

The decomposition of CAC takes place in two stages. The first stage, which occurs at a temperature ranging from 29.99°C to 147.48°C involves the loss of moisture present in the sample with an approximate weight loss of 11.401% [23,24]. The maximum rate of weight loss occurred at the second stage ranging from 147.48°C to 903.11°C with the percentage loss of 41.69%. This step is related to the slow thermal decomposition of organic carbon structure of hemicellulose, cellulose, or lignin [23,24].

The decomposition of OPFAD takes place in three stages. The initial degradation ranging from 28.94°C to 139.64°C is attributed to the weight loss of moisture in the sample at 6.850% [22]. The second degradation around

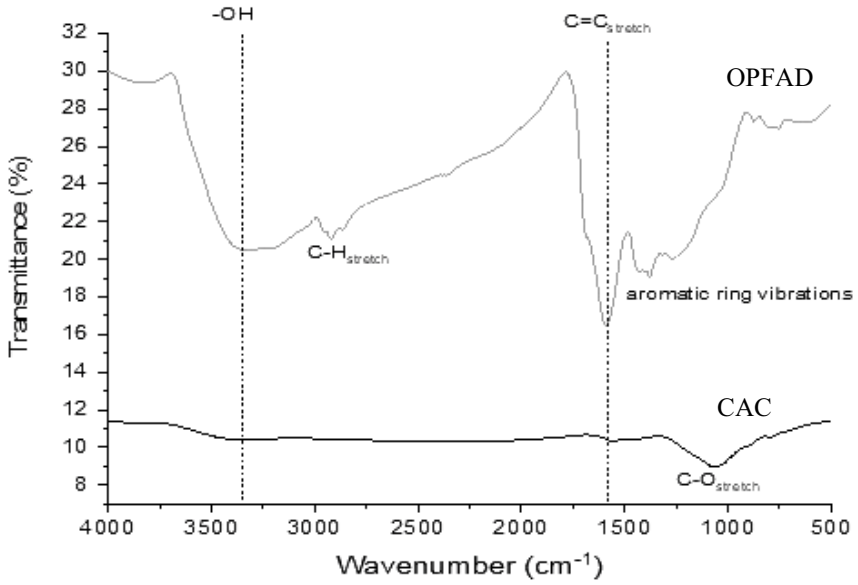

Fig. 1. FTIR spectra for CAC and OPFAD.

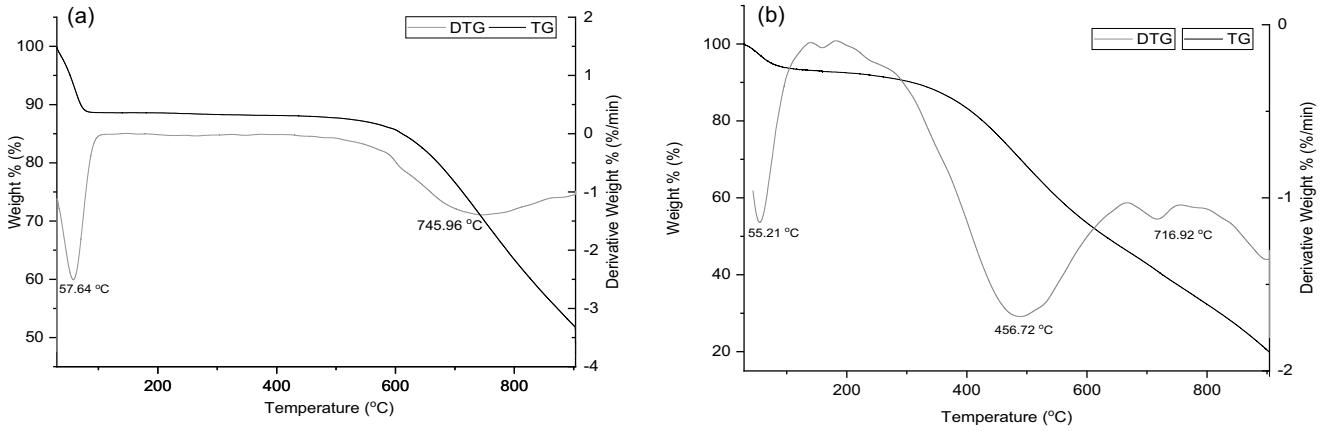

Fig. 2. TG and DTG curves for (a) CAC and (b) OPFAD.

139.64°C–668.04°C is the maximum rate of weight loss of 47.034%. The broad DTG curve indicates the release of volatile compounds resulting from the decomposition of hemicellulose and cellulose [22,23]. Above 668.04°C, the OPFAD samples exhibited a weight loss up to 904.13°C, which is related with the steady decomposition of lignin remained in solid residue or char with a percentage loss of 27.357% [25,26].

Based on the previous studies [18,19,27], raw OPF showed an initial weight loss at a temperature range between 50°C and 150°C due to the evaporation of water in cellulose fibers. In contrast, the temperature range between 150°C and 250°C was due to the depolymerization of non-celluloses, including hemicellulose and lignin. According to Al-Lagtah et al. [18], before the major peak, there was a small broad peak at 280°C indicates the presence of low molecular weight compounds, hemicellulose, and lignin. Owolabi et al. [27] stated that the raw OPF degraded by 70% when the samples are further heating beyond 400°C. The raw OPF samples maintained a high residual mass due to the presence of lignin and ashes within the samples. When the samples were burnt, the ashes started to regenerate and cause only a small reduction of the samples' weight.

3.3. N_2-BET analysis

Surface area and porosity are the significant characteristics for the adsorbent. The BET surface area, total pore volume, and average pore diameter of CAC, OPF, and OPFAD are listed in Table 1 while Fig. 3 shows the plot of N_2 adsorption–desorption isotherm for OPFAD.

According to BET analysis, there was an improvement in the BET surface area, total pore volume and average pore diameter from 2.0917 m^2 g^{-1}, 0.002148 cm^3 g^{-1}, and 4.10735 nm (for OPF) to 2.7273 m^2 g^{-1}, 0.003112 cm^3 g^{-1}, and 4.56361 nm (for OPFAD), respectively, after chemical activation. The pore structure of activated carbon can be affected by the activation temperature as it is one of the critical parameters. When the activation temperature increases, the reaction rate between the activating agent and carbons also increases [28]. Based on the average pore diameter, OPF (4.11 nm), and OPFAD (4.56 nm) can be classified as mesoporous. In comparison, CAC (1.75 nm) can be classified as microporous based on the International Union of Pure and Applied Chemistry (IUPAC). The IUPAC classified the pores as macropores (>50 nm diameter), mesopores (2–50 nm diameter), and micropores (<2 nm diameter) [29].

Table 1
BET summary for CAC, OPF, and OPFAD

Sample	BET surface area (m^2 g^{-1})	Total pore volume (cm^3 g^{-1})	Average pore diameter (nm)
CAC	530.612	0.53	1.74896
OPF	2.0917	0.002148	4.10735
OPFAD	2.7273	0.003112	4.56361

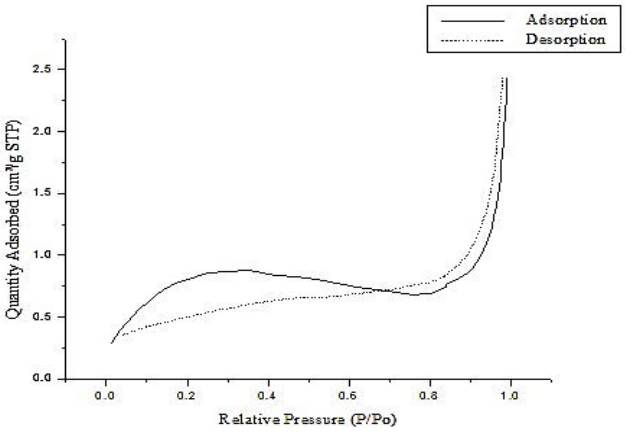

Fig. 3. N_2 adsorption–desorption isotherm plot for OPFAD.

3.4. SEM/EDX analyses

SEM analysis was carried out to study the morphology of OPF and OPFAD while EDX analysis was done to examine the main element present in OPF and OPFAD. Fig. 4 depicts SEM micrographs at 3,000× magnification

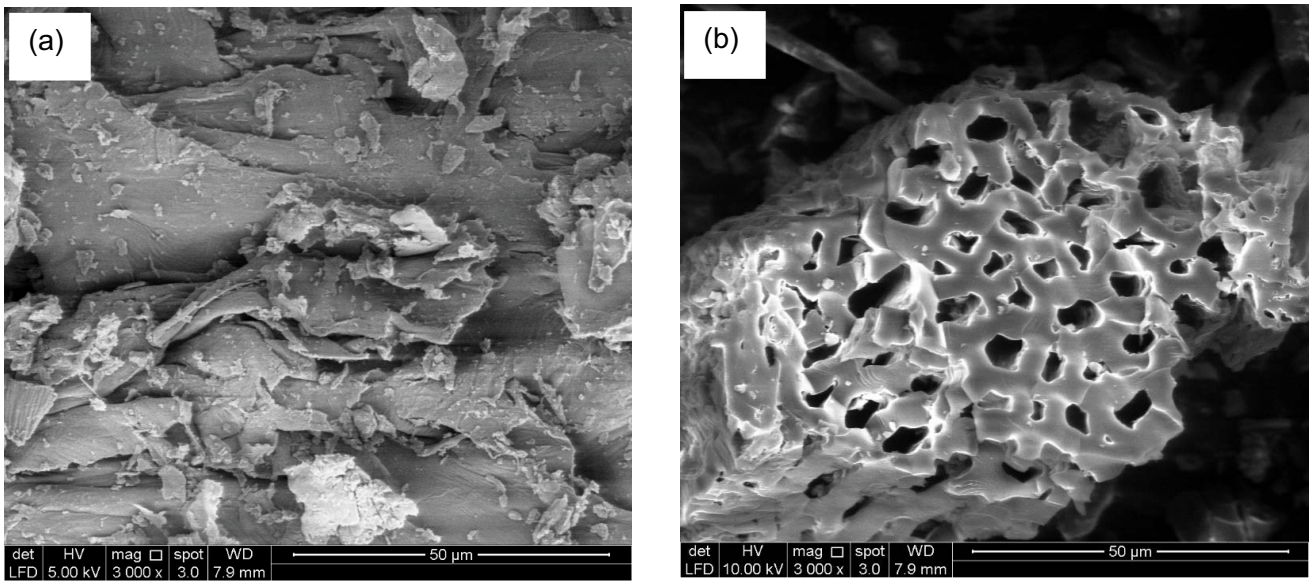

Fig. 4. SEM micrographs (3,000× magnification) of (a) OPF and (b) OPFAD.

and their EDX spectra. As observed, the SEM images of OPFAD showed the existence of a larger pore size as compared to OPF, which is concurrence with the result obtained from BET analysis.

From Fig. 5, it shows that the samples are mainly composed of carbon and oxygen. Table 2 indicates the presence of C (53.72%), O (46.28%), and C (78.25%), O (16.80%) in samples of OPF and OPFAD, respectively. Notable differences were observed between the carbon content of OPF and OPFAD.

Table 2
EDX elemental analyses for OPF and OPFAD

	OPF		OPFAD	
Element	Weight (%)	Atomic (%)	Weight (%)	Atomic (%)
C K	53.72	60.73	78.25	84.70
O K	46.28	39.27	16.80	13.65
KK	–	–	4.94	1.64
Total	100.00		100.00	

3.5. CHN analysis

The elemental compositions of CAC, OPF, and OPFAD are presented in Table 3. As observed, OPFAD, compared to OPF and CAC, showed significant differences in the proportions of the different elements. Thus, the conversion of OPF into OPFAD led to an increased carbon (41.07%–57.82%) and nitrogen (1.00%–1.20%) content, as well as reduced hydrogen (5.63%–3.74%) content. The result obtained corresponded well with the data attained through BET, SEM, and EDX analyses.

Table 3
CHN elemental compositions of CAC, OPF, and OPFAD

Sample	C	H	N
CAC	41.07	1.01	0.55
OPF	41.07	5.63	1.00
OPFAD	57.82	3.74	1.20

C, H, and N: %.

3.6. Effect of adsorbent dosage

The effect of adsorption dosage was investigated by ranging the OPFAD dosage from 0.01 to 5.0 g. Fig. 6 shows that the percentage removal increases with a higher amount of OPFAD dosage, which was due to the increment of accessibility for the adsorption surface area and active sites in OPFAD [5]. The percentage removal increased from 71.71% to 81.90% as the adsorbent dosage risen from 0.01 to 0.1 g. It was also seen that the percentage of removal started to drop from 0.5 g (72.1%) to 5 g (41.42%). However, adsorbed dye quantity (mg of MB) per gram of adsorbent (q_e) decreased (from 72.27 to 9.13 mg g^{-1}) with the increase in adsorbent dosage. The explanation for this is that as the OPFAD dosage increases more than 0.1 g, there would be excess of unutilized adsorption sites due to the fixed concentration of MB used in the adsorption study. More specifically, increasing the loading of OPFAD beyond 0.1 g would enhance unused available adsorption sites within OPFAD, consequently decreasing the adsorption capacity value. Thus, relatively higher amount of OPFAD in the solution results in reduced distances among the OPFAD particles, which makes majority of binding sites unoccupied [5]. Shakoor and Nasar [30] pointed out that the reduction in adsorption capacity with increased adsorbent dosage could be related to the inter-particles interaction (namely aggregation or overcrowding), resulting

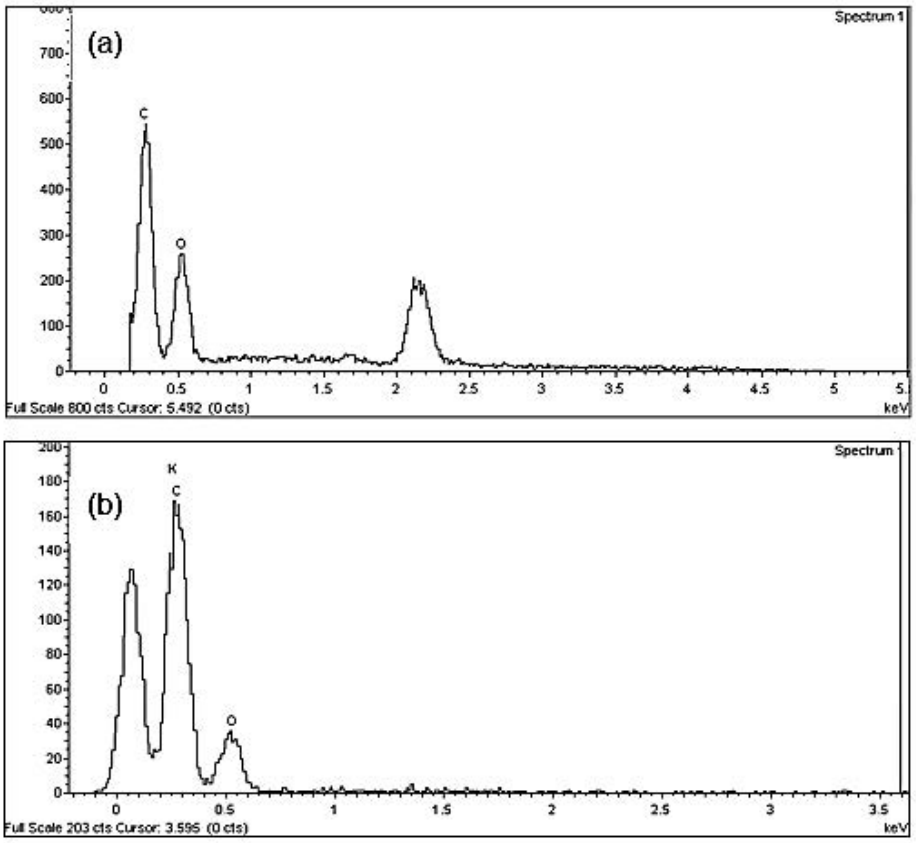

Fig. 5. EDX spectra for (a) OPF and (b) OPFAD.

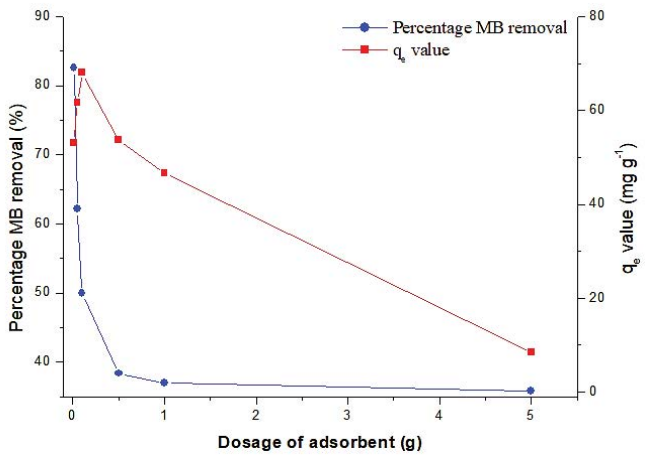

Fig. 6. Effect of dosage of adsorbent (MB concentration = 100 ppm, volume = 25 mL, and time = 24 h) on MB removal and q_e value of OPFAD.

in reduced available total surface area. From the results, the optimum dosage of OPFAD was determined at 0.1 g.

3.7. pH_{pzc} and the effect of pH

The pH_{pzc} indicate that the pH of the adsorbent where the adsorbent net surface charge is corresponding to zero. Pirbazari et al. [31] reported that cationic dye adsorption is favored at pH > pH_{pzc}, due to functional groups like OH^- and COO^- are present. In contrast, the anionic dye adsorption is favored at pH < pH_{pzc} as the adsorbent surface is positively charged. The graph of pH_{final} vs. $pH_{initial}$ was plotted, as shown in Fig. 7. The intersection of the curves with the straight line is known as the endpoint of the pH_{pzc} with a value of 6.44 for OPFAD. Thereby, this indicated that the OPFAD surface was positively charged at pH < 6.44 and negatively charged at pH > 6.44 [16].

Fig. 8 shows the effect of pH on MB removal by OPFAD and its q_e value. It was observed that pH gives a notable influence on the adsorption process. MB is a cationic dye and exists in the form of positive charge ions in an aqueous solution. The surface charge on the adsorbent primarily influences the degree of adsorption of the charged particle onto the adsorbent surface; in other words, it is influenced by the pH of the solution [31]. As shown in Fig. 8, the removal percentage was minimum at pH 4 (64.4%) and maximum at pH 12 (84.31%). Due to the presence of excess H^+ ions competing with the cation groups on the dye for adsorption sites, it will lower the percentage removal of MB at acidic pH (pH < pH_{pzc}) [4,31]. On the other hand, at higher solution pH (pH > pH_{pzc}), the OPFAD possibly be negatively charged and enhance the positively charged dye cations through electrostatic forces of attraction [16,31]. From the results above, the optimum pH of OPFAD was determined at pH 12.

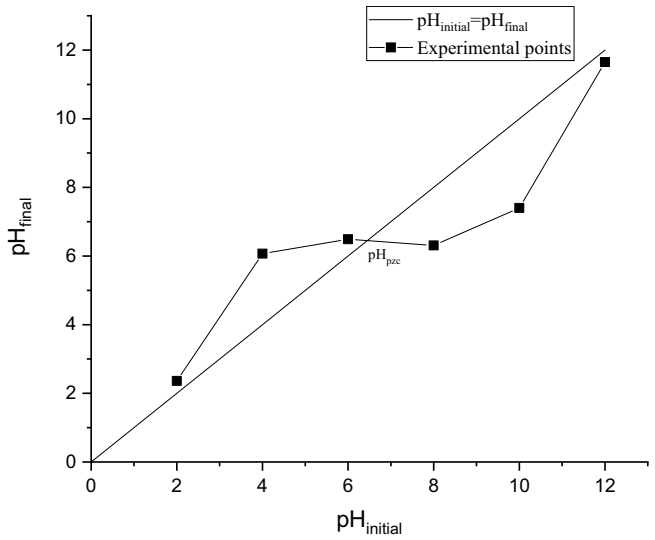

Fig. 7. pH_{pzc} (adsorbent dosage = 0.1 g, volume = 100 mL, and time = 48 h) of OPFAD.

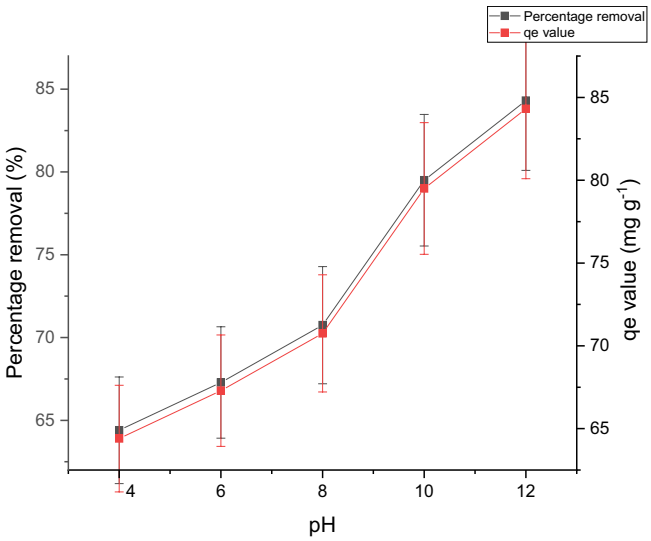

Fig. 8. Effect of pH (adsorbent dosage = 0.1 g, MB concentration = 100 ppm, volume = 100 mL, and time = 24 h) on MB removal and q_e value of OPFAD.

3.8. Effect of contact time

The contact time is inevitably a fundamental parameter in all transfer phenomena such as adsorption. The effect of the contact time of OPFAD on the removal of MB is shown in Fig. 9. From the obtained result, it is noticeable that the removal of MB increased with prolonged contact time. This phenomenon was observed due to the vacancies of active sites on the adsorbent surface and high solution concentration [2]. It was noted that after 24 h contact time, the percentage of removing MB was the highest (81.9%). Therefore, the contact time 24 h was selected for further study.

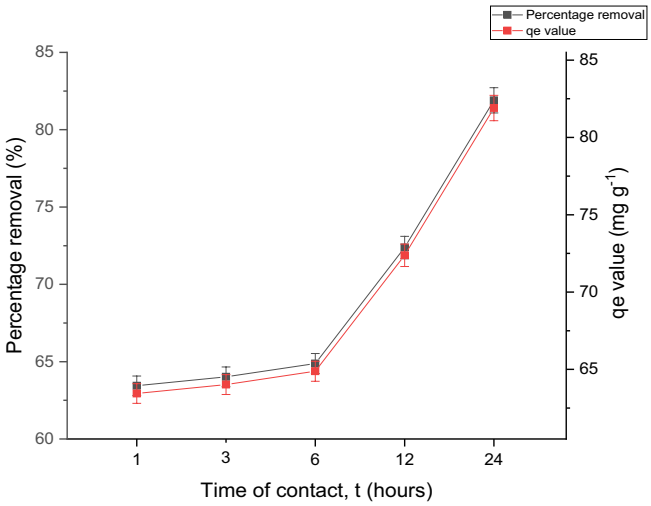

Fig. 9. Effect of contact time (adsorbent dosage = 0.1 g, MB concentration = 100 ppm, and volume = 100 mL) on MB removal and q_e value of OPFAD.

3.9. Effect of initial MB dye concentration

One of the critical factors for effective adsorption is to consider the rate of adsorption of the initial concentration of the adsorbate. The effect of initial concentration on the adsorption and dye removal efficiency is presented in Fig. 10. The result indicates that the percentage removal and actual amount of MB dye adsorbed per unit mass of OPFAD increased with an increase in the initial MB dye concentration. This is because as the initial dye concentration increases, the driving force of the concentration gradient will also increase [32]. The percentage removal for MB dye risen from 69.9% to 82.8% as the MB concentration increased from 5 to 40 ppm. As observed, there is a decrease in percentage removal from 60 ppm (82.2%) to 100 ppm (81.9%). This result may be attributed to the lack of available active sites required for the high initial concentration of the dyes [4]. The adsorption sites absorbed the available solute more quickly at low concentration [4,33].

3.10. Adsorption isotherms

The equilibrium of adsorption for the solid–liquid system is one of the prime physico-chemical aspects in describing adsorption behavior [33]. In this study, three models of Langmuir, Freundlich, and Temkin isotherm are evaluated.

The Langmuir isotherm is based on the presumption of monolayer adsorption onto a surface containing adsorption sites, whereby once the system achieved saturation, there will be no further adsorption occurred [34]. This model is the most widely used two-parameter equation, generally expressed in the form by the following Eq. (3) [33]:

$$\frac{C_e}{Q_e} = \frac{1}{Q_m K_L} + \frac{1}{Q_m} C_e \tag{3}$$

where C_e is the equilibrium concentration of the adsorbate (mg L^{-1}), Q_e is the amount of the adsorbate per unit mass of adsorbent (mg g^{-1}), K_L is the Langmuir adsorption constant (L mg^{-1}), and Q_m is the theoretical maximum adsorption capacity (mg g^{-1}).

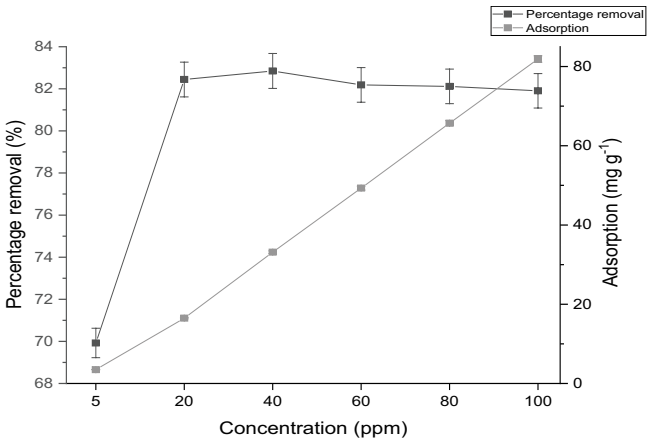

Fig. 10. Effect of initial concentration (adsorbent dosage = 0.1 g, volume = 100 mL, and time = 24 h) on MB removal and adsorption of OPFAD.

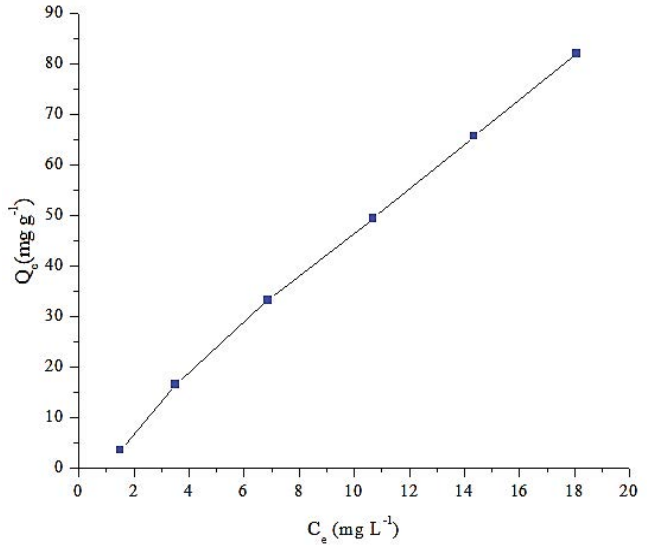

Fig. 11. Equilibrium adsorption isotherm of MB onto OPFAD.

The vital characteristic of the Langmuir equation is it can be expressed in terms of a dimensionless separation factor R_L, which is defined as Eq. (4) [33].

$$R_L = \frac{1}{1 + K_L C_0} \tag{4}$$

where K_L is the Langmuir adsorption constant (L mg^{-1}), and C_0 is the initial dye concentration (mg L^{-1}). The R_L value indicates the type of the isotherm to be either favorable ($0 < R_L < 1$), unfavorable ($R_L > 1$), linear ($R_L = 1$), or irreversible ($R_L = 0$).

The Freundlich isotherm, on the other hand, takes heterogeneous systems into account and is not restricted to the formation of the monolayer [35]. Eq. (5) gives the well-known logarithmic form of the Freundlich isotherm [5].

$$\ln Q_e = \ln K_F + \frac{1}{n} \ln C_e \tag{5}$$

where K_F (L mg^{-1}) and n are Freundlich constants. K_F is defined as an adsorption or distribution coefficient representing the amount of the adsorbate adsorbed on an adsorbent for a unit equilibrium concentration. At the same time, n indicates how favorable the adsorption process.

The slope of $1/n$ ranging between 0 and 1 is a measure of adsorption intensity or surface heterogeneity, becoming more heterogeneous as its value gets closer to zero. A value for $1/n$ below 1 indicates a normal Langmuir isotherm, while $1/n > 1$ is indicative of cooperative adsorption [36].

Temkin isotherm is a model that describes the effects of indirect adsorbate–adsorbate interactions and suggests that the heat of bio-sorption of molecules on the layer would decrease linearly instead of logarithmic with coverage [5]. The derivation in Temkin isotherm has been used in the form, as shown in Eq. (6) [37]:

$$q_e = B \ln A + B \ln C_e \tag{6}$$

where $B = -RT/b$, b is the Temkin constant related to the heat of adsorption (J mol^{-1}), A is the Temkin isotherm constant (L g^{-1}), R is the gas constant (8.314 J mol^{-1} K^{-1}), and T is the absolute temperature (K).

Fig. 11 represents Q_e vs. C_e graph. Langmuir, Freundlich, and Temkin isotherms for adsorption of MB on OPFAD are shown in Figs. 12–14, respectively.

Isotherm parameters and the determination coefficients were calculated and summarized in Table 4. As shown in the table, the Langmuir isotherm with the correlation coefficient of 0.9997 represents a better fit of experimental data than the Freundlich model (R^2 = 0.9975) and Temkin model (R^2 = 0.9661). It indicates that monolayer adsorption of MB dye takes place on the homogeneous surface of OPFAD. This finding was similar to other studies, for example, Langmuir isotherm was found to fit well with the experimental data in the adsorption of methylene blue by coconut bunch waste [37], apricot stones activated carbon [4], and karanj fruit hulls activated carbon [9].

Based on previous studies, the adsorption of methylene blue onto apricot stones and bamboo-based activated carbon correspondingly follow the Langmuir isotherm model as it gives the best fit for the equilibrium data [4,38]. Moreover, Kannan and Sundaram [39] reported on the kinetics and mechanism of removal of methylene blue by adsorption onto various carbons, where the adsorption behavior of methylene blue onto the activated carbon prepared from bamboo dust, coconut shell, groundnut shell, rice husk, and straw are also best described by a monolayer Langmuir type isotherm.

The amount of computed maximum monolayer capacity for the removal of MB from aqueous media by Langmuir model was found to be 95.24 mg g^{-1}. Moreover, the values of the dimensionless constant R_L (0.168) indicate that the adsorption is favorable and somewhat irreversible.

The adsorption of Gibbs free energy ($\Delta G°$) can be calculated using Eq. (7) [5]:

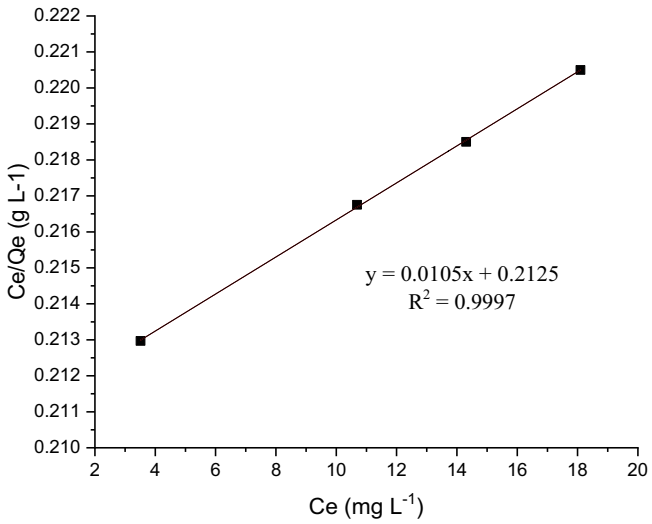

Fig. 12. Langmuir isotherm for adsorption of MB on OPFAD.

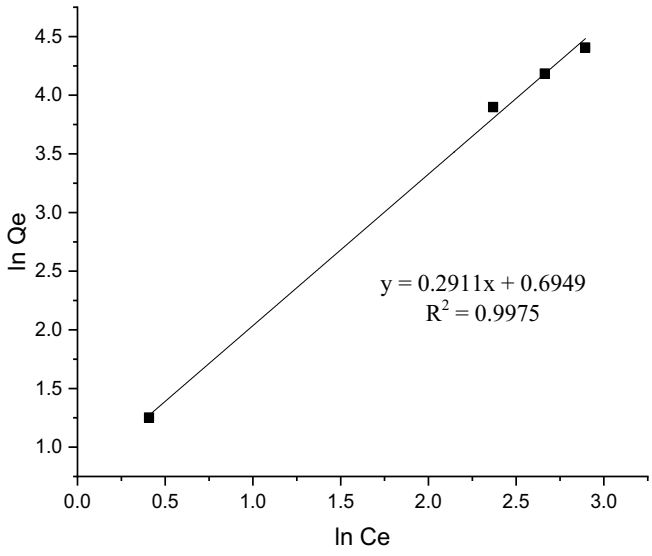

Fig. 13. Freundlich isotherm for adsorption of MB on OPFAD.

$$\Delta G^\circ = -RT\ln K_L^o \tag{7}$$

where R is the universal gas constant (8.314 J K^{-1} mol^{-1}), T is the temperature in Kelvin and K_L^o is the thermodynamic equilibrium constant of Langmuir isotherm for the adsorption process. K_L^o can be obtained through a calculation using data from Langmuir isotherm and expressed as Eq. (8) [5]:

$$K_L^o = K_L\left(\text{L mg}^{-1}\right)\times 1{,}000\left(\text{mg g}^{-1}\right)\times M_{\text{MB}}\left(\text{g mol}^{-1}\right)\times C^o\left(\text{mol L}^{-1}\right) \tag{8}$$

where C^o = 1, M_{MB} = 319.85 g mol^{-1} is the MB molar mass, and the factor of 1,000 allows converting g to mg.

The negative value of ΔG° (–24.36 kJ mol^{-1}) indicated the spontaneity of the adsorption process and energy generation during the process [9,16]. Thus, MB molecules are physically adsorbed onto the surface of OPFAD.

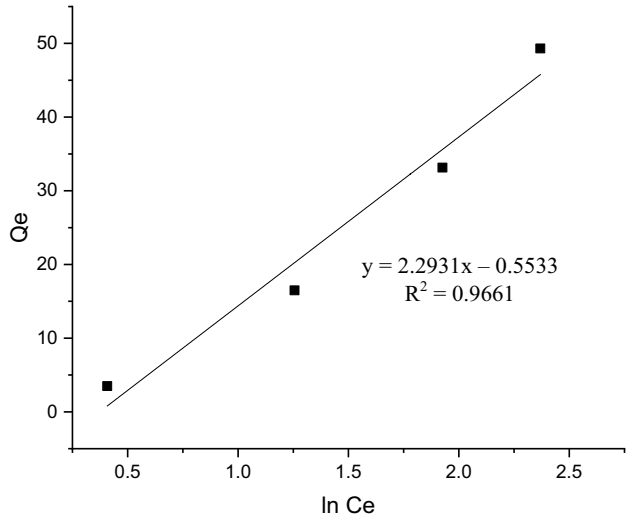

Fig. 14. Temkin isotherm for adsorption of MB on OPFAD.

3.11. Adsorption kinetics

The study of adsorption kinetics is vital as the rate of adsorption, and the mechanism of adsorption can be obtained from kinetic studies. In order to evaluate adsorption kinetics, three common models were applied to the experimental data obtained from the adsorption process. These are pseudo-first-order, pseudo-second-order kinetic models, and Weber's intraparticle diffusion model as shown in Eqs. (9), (11), and (12), respectively [40–42].

$$\ln\left(Q_e - Q_t\right) = \ln Q_e - k_1 t \tag{9}$$

Eq. (9) can be rearranged in a non-linearized form as depicted in Eq. (10):

$$Q_t = Q_e\left(1 - e^{-k_1 t}\right) \tag{10}$$

$$\frac{t}{Q_t} = \frac{1}{h} + \frac{1}{Q_e}t,\ h = k_2 Q_e^2 \tag{11}$$

$$Q_t = K_p t^{1/2} \tag{12}$$

where k_1 (min^{-1}) and k_2 (g mg^{-1} min^{-1}) are the adsorption rate constants of pseudo-first- and pseudo-second-order adsorptions, respectively; Q_e and Q_t are the amounts of dyes adsorbed at equilibrium and time t (mg g^{-1}); h is the initial rate of adsorption (mg g^{-1} min^{-1}), and K_p is the intraparticle diffusion rate constant (mg g^{-1} min$^{-1/2}$).

The adsorption kinetics plots are shown in Fig. 15, and all the kinetic parameters determined are listed in Table 5. Since calculated determination coefficients are closer to unity for the pseudo-second-order kinetic model than the pseudo-first-order kinetic model (0.9995 vs. 0.7856) and

Table 4
Langmuir, Freundlich. and Temkin constants for the adsorption of MB on OPFAD

Langmuir				Freundlich			Temkin		
Q_m	K_L	R_L	R^2	K_F	$1/n$	R^2	B	A	R^2
95.24	0.04941	0.168	0.9997	2.004	0.2911	0.9975	2.2931	0.7856	0.9661

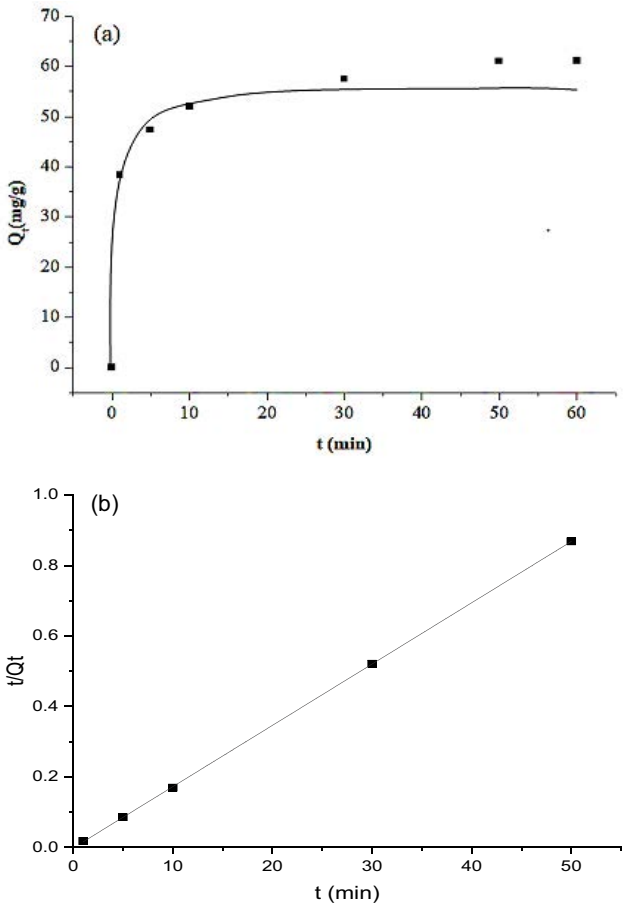

Fig. 15. (a) Pseudo-first-order (non-linear) and (b) pseudo-second-order (linear) kinetic models for the adsorption of MB on OPFAD.

calculated adsorption capacity from pseudo-second-order model is closer to the experimental q_e value (61.13 mg g^{-1}). Thus, the system principally follows the second-order rate model. Based on previous studies, the adsorption of methylene blue onto the apricot stone and bamboo-based activated carbon similarly follows the pseudo-second-order model with R^2 values of 0.999 and >0.99, respectively [4,38]. Additionally, the adsorption behavior of methylene blue onto the activated carbons fabricated from bamboo dust, coconut shell, groundnut shell, rice husk, and straw suitably fitted the first order with intra-particle diffusion as one of the rate-determining steps [39].

A better fit with the pseudo-second-order kinetic model suggests that the adsorption rate is dependent more on the availability of the adsorption sites rather than the concentration of the MB dye [16]. Moreover, it also suggests that physisorption is the possible rate-determining step that controls the adsorption process; as such, the adsorption rate of MB and number of active sites available on the OPFAD surface show a proportional relationship [4,9].

Fig. 16 shows the linear plot of $t^{1/2}$ vs. Q_t. If the regression of $t^{1/2}$ vs. Q_t is linear and passes through the origin, then intraparticle diffusion is the sole rate-limiting step [43]. In previous studies, such plots may present a multilinearity, which suggests that two or more steps occur [39,44,45]. In the present study, the plot also did not pass through the origin, indicating that although intraparticle diffusion was involved in the adsorption process, it was not the sole rate-controlling step. This also confirms that adsorption of MB on the adsorbent was a multi-step process involving external surface adsorption or instantaneous adsorption stage and intraparticle diffusion into the interior [45,46]. Fig. 16 suggests that the adsorption process proceeds by surface adsorption and the second phase indicates that intraparticle diffusion is the rate-limiting step. According to Cheung et al. [47], this could be explained that there were two processes that concurred the rate of dye adsorption, but only one was the rate-limiting in any time range. Since the dual nature of intraparticle diffusion plot, it confirms the presence of both surface adsorption and intraparticle diffusion [39,44].

3.12. Adsorption mechanism

The results of different factors on MB dye adsorption, adsorption kinetics, and isotherm are summarized. The above analysis shows that the adsorption of methylene blue onto OPFAD was a complicated process, involving multiple

Table 5
Pseudo-first-order (non-linear) and pseudo-second-order (linear) model constants for the adsorption of MB on OPFAD

Pseudo-first-order			Pseudo-second-order		
k_1 (min^{-1})	R^2	Q_e (mg g^{-1})	k_2 (g mg^{-1} min^{-1})	R^2	Q_e (mg g^{-1})
0.0103	0.7856	47.12	0.0528	0.9995	58.14

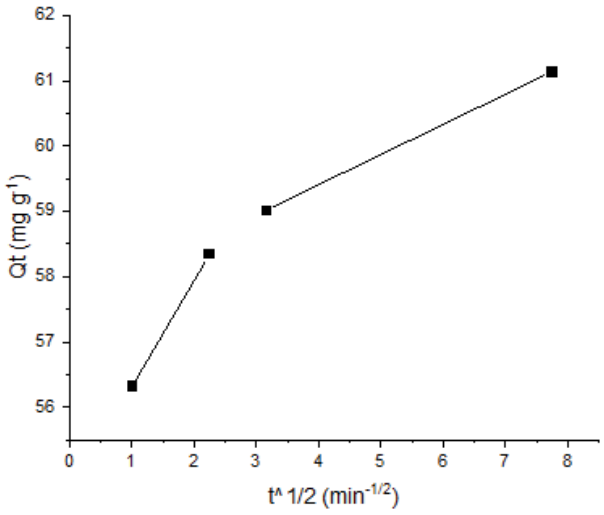

Fig. 16. Weber's intraparticle diffusion model.

steps and various interactions. According to the results of the pH effect, electrostatic interaction existed between OPFAD and MB dye. The molecular bonding could occur between MB dye and OPFAD through surface complexion [48]. MB formed MB^+ ions and attracted to the OPFAD. However, electrostatic interaction is not the sole mechanism. Meanwhile, Langmuir isotherm suggests that adsorption occurred on monolayer basis onto a surface containing adsorption sites [34].

Moreover, the pseudo-second-order model could fit the kinetics data of MB adsorption onto OPFAD, suggesting that chemisorption interactions play a dominant role during the adsorption process. Besides, Weber's model indicated the presence of both surface adsorption and intraparticle diffusion. Hydrogen bond or π–π stacking interaction between MB and OPFAD may also exist during the adsorption process. This result was consistent with the analysis of the OPFAD by FTIR, which showed the presence of those functional groups. The two benzene rings contained in MB dye quickly form π–π stacking interaction with the aromatic rings in the OPFAD [48].

The interaction between OPFAD and MB is referred to various mechanisms, including electrostatic interaction, monolayer adsorption, chemisorption interactions, surface diffusion, intraparticle diffusion, hydrogen bonding, and π–π binding. The recommended mechanism diagram is depicted in Fig. 17.

4. Conclusion

This study explored the potential of OPF as a low-cost precursor of OPFAD. OPFAD presents a mesopores pore diameter with a BET average pore diameter of 4.56 nm. The operating parameters for the maximum adsorption were adsorbent dosage (0.1 g/100 mL), dye concentration (40 ppm), and time contact (24 h). Removal of MB dye is pH-dependent and maximum removal was attained at pH 12. The Langmuir isotherm model best fitted the adsorption equilibrium data with a $\Delta G° = -24.36$ kJ mol^{-1}. The negative $\Delta G°$ values indicated that the adsorbent of dye onto OPFAD was feasible and spontaneous. Meanwhile, the excellent correlation coefficient from adsorption experiment suggested that the adsorption kinetics could be best described by the pseudo-second-order kinetic model which

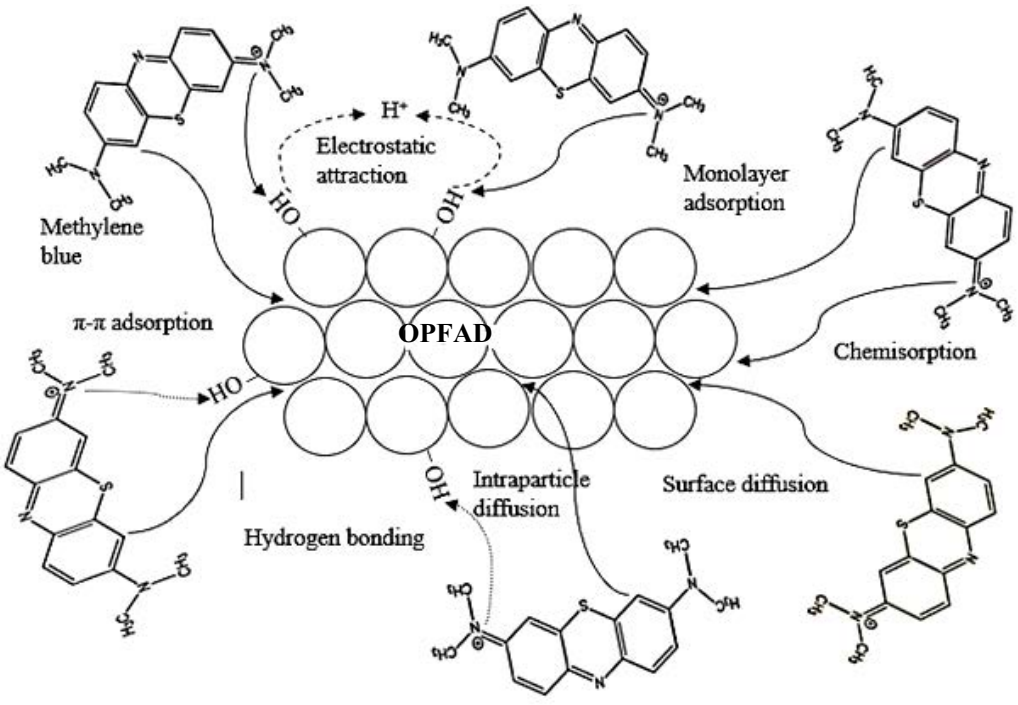

Fig. 17. Schematic illustrated mechanism diagram of MB adsorption by OPFAD.

confirmed that the adsorption rate dependent on the availability of adsorption sites rather than MB dye concentration. On the whole, these results showed that OPFAD is an effective adsorbent and can act as an alternative to CAC for MB dye adsorption.

Acknowledgments

This research was financially supported by the USM Research University Incentive (RUI) Grant: 1001/PKIMIA/8011077 and the external grant funded by NAHRIM (304/PKIMIA/650968/I136 and 304/PKIMIA/650973/I136).

Symbols

°C	—	Degree of Celcius
%	—	Percentage
$\Delta G°$	—	Gibbs free energy change, kJ mol^{-1}
C_e	—	Equilibrium concentration, mg L^{-1}
cm	—	Centimeter
C_0	—	Initial concentration, mg L^{-1}
g	—	Gram
h	—	Hour
K	—	Kelvin
K_F	—	Freundlich constant related to maximum adsorption capacity, mg g^{-1}
K_L	—	Langmuir adsorption constant, L mg^{-1}
K_p	—	Intraparticle diffusion rate constant, mg g^{-1} min$^{-1/2}$
L	—	Liter
L g^{-1}	—	Liter per gram
mg	—	Milligram
mg g^{-1}	—	Milligram per gram
min	—	Minute
mL	—	Milliliter
mL min^{-1}	—	Milliliter per minute
nm	—	Nanometer
pH_{pzc}	—	pH point of zero charge
ppm	—	Parts per million
q_e	—	Adsorption capacity at equilibrium, mg g^{-1}
Q_m	—	Theoretical maximum adsorption capacity, mg g^{-1}
Q_t	—	Adsorption capacity at time, mg g^{-1}
R	—	Gas constant, 8.314 J mol^{-1} K^{-1}
R^2	—	Correlation coefficient
R_L	—	Dimensionless factor (from Langmuir)
rpm	—	Revolutions per minute
T	—	Temperature, K
V	—	Volume, L
W	—	Weight, g
w/w	—	Weight per weight

References

[1] M. Auta, B.H. Hameed, Preparation of waste tea activated carbon using potassium acetate as an activating agent for adsorption of acid blue 25 dye, Chem. Eng. J., 171 (2011) 502–509.
[2] D. Pathania, S. Sharma, P. Singh, Removal of methylene blue by adsorption onto activated carbon developed from ficus carica bast, Arabian J. Chem., 10 (2017) S1445–S1451.
[3] H.D. Setiabudi, R. Jusoh, S.F.R.M. Suhaimi, S.F. Masrur, Adsorption of methylene blue ontooil palm (*Elaeis guineensis*) leaves: process optimization, isotherm, kinetics and thermodynamic studies, J. Taiwan Inst. Chem. Eng., 63 (2016) 363–370.
[4] C. Djilani, R. Zaghdoudi, F. Djazi, B. Bouchekima, A. Lallam, A. Modarressi, M. Rogalski, Adsorption of dyes on activated carbon prepared from apricot stones and commercial activated carbon, J. Taiwan Inst. Chem. Eng., 53 (2015) 112–121.
[5] C.H.C. Tan, S. Sabar, M.H. Hussin, Development of immobilized microcrystalline cellulose as an effective adsorbent for methylene blue dye removal, S. Afr. J. Chem. Eng., 26 (2018) 11–24.
[6] A. Nasrullah, B. Saad, A.H. Bhat, A.S. Khan, M. Danish, M.H. Isa, A. Naeem, Mangosteen peel waste as a sustainable precursor for high surface area mesoporous activated carbon: characterization and application for methylene blue removal, J. Cleaner Prod., 211 (2019) 1190–1200.
[7] M. Danish, T. Ahmad, S. Majeed, M. Ahmad, L. Ziyang, Z. Pin, S.S. Iqubal, Use of banana trunk waste as activated carbon in scavenging methylene blue dye: kinetic, thermodynamic, and isotherm studies, Bioresour. Technol. Rep., 3 (2018) 127–137.
[8] M. Danish, T. Ahmad, R. Hashim, N. Said, M.N. Akhtar, J. Mohamad-Saleh, O. Sulaiman, Comparison of surface properties of wood biomass activated carbons and their application against rhodamine B and methylene blue dye, Surf. Interfaces, 11 (2018) 1–13.
[9] M.A. Islam, S. Sabar, A. Benhouria, W.A. Khanday, M. Asif, B.H. Hameed, Nanoporous activated carbon prepared from karanj (*Pongamia pinnata*) fruit hulls for methylene blue adsorption, J. Taiwan Inst. Chem. Eng., 74 (2017) 96–104.
[10] A.M. Aljeboree, A.N. Alshirifi, A.F. Alkaim, Kinetics and equilibrium study for the adsorption of textile dyes on coconut shell activated carbon, Arabian J. Chem., 10 (2017) S3381–S3393.
[11] M. Rafatullah, T. Ahmad, A. Ghazali, O. Sulaiman, M. Danish, R. Hashim, Oil palm biomass as a precursor of activated carbons: a review, Crit. Rev. Environ. Sci. Technol., 43 (2013) 1117–1161.
[12] R. Diyanilla, T.S. Hamidon, L. Suryanegara, M.H. Hussin, Overview of pretreatment methods employed on oil palm biomass in producing value-added products: a review, Bioresources, 15 (2020), 9935–9997.
[13] J.M. Salman, V.O. Njoku, B.H. Hameed, Batch and fixed-bed adsorption of 2,4-dichlorophenoxyacetic acid onto oil palm frond activated carbon, Chem. Eng. J., 174 (2011) 33–40.
[14] J.M. Salman, B.H. Hameed, Effect of preparation conditions of oil palm fronds activated carbon on adsorption of bentazon from aqueous solutions, J. Hazard. Mater., 175 (2010) 133–137.
[15] M. Danish, T. Ahmad, R. Hashim, M.R. Hafiz, A. Ghazali, O. Sulaiman, S. Hiziroglu, Characterization and adsorption kinetic study of surfactant treated oil palm (*Elaeis guineensis*) empty fruit bunches, Desal. Water Treat., 57 (2016) 9474–9487.
[16] V.O. Njoku, M.A. Islam, M. Asif, B.H. Hameed, Preparation of mesoporous activated carbon from coconut frond for the adsorption of carbofuran insecticide, J. Anal. Appl. Pyrolysis, 110 (2014) 172–180.
[17] S. Tian, Z. Zhang, X. Zhang, K. Ostrikov, Capacitative deionization using commercial activated carbon fiber decorated with polyaniline, J. Colloid Interface Sci., 537 (2019) 247–255.
[18] N.M.A. Al-Lagtah, A.H. Al-Muhtaseb, M.N.M. Ahmad, Y. Salameh, Chemical and physical characteristics of optimal synthesised activated carbons from grass-derived sulfonated lignin versus commercial activated carbons, Microporous Mesoporous Mater., 225 (2016) 504–514.
[19] L.W. Lai, A. Idris, Disruption of oil palm trunks and fronds by microwave-alkali pretreatment, Bioresources, 8 (2013) 2792–2804.
[20] S.R.A.M. Rasli, I. Ahmad, A.M. Lazim, A. Hamzah, Extraction and characterization of cellulose from agricultural residue-oil palm fronds, Malaysian J. Anal. Sci., 21 (2017) 1065–1073.
[21] N.A. Nordin, O. Sulaiman, R. Hashim, M.H.M. Kassim, Oil palm frond waste for the production of cellulose nanocrystals, J. Phys. Sci., 28 (2017) 115–126.
[22] M.H. Hussin, A.A. Rahim, M.N. Mohamad Ibrahim, N. Brosse, Physicochemical characterization of alkaline and ethanol

organosolv lignins from oil palm (*Elaeis guineensis*) fronds as phenol substitutes for green material applications, Ind. Crops Prod., 49 (2013) 23–32.
[23] C. Saka, BET, TG–DTG, FT-IR, SEM, iodine number analysis and preparation of activated carbon from acorn shell by chemical activation with $ZnCl_2$, J. Anal. Appl. Pyrolysis, 95 (2012) 21–24.
[24] A. Bazan, P. Nowicki, P. Półrolniczak, R. Pietrzak, Thermal analysis of activated carbon obtained from residue after supercritical extraction of hops, J. Therm. Anal. Calorim., 125 (2016) 1199–1204.
[25] A. Mamaní, M.F. Sardella, M. Giménez, C. Deiana, Highly microporous carbons from olive tree pruning: optimization of chemical activation conditions, J. Environ. Chem. Eng., 7 (2019) 102830, doi: 10.1016/j.jece.2018.102830.
[26] A.A. Salema, M.T. Afzal, F. Motasemi, Is there synergy between carbonaceous material and biomass during conventional pyrolysis? A tg-ftir approach, J. Anal. Appl. Pyrolysis,105 (2014) 217–226.
[27] A.F. Owolabi, A. Ghazali, H.A. Khalil, A. Hassan, R. Arjmandi, M.N. Fazita, M.M. Haafiz, Isolation and characterization of microcrystalline cellulose from oil palm fronds using chemomechanical process, Wood Fiber Sci., 48 (2016) 1–11.
[28] K. Sun, J. Chun Jiang, Preparation and characterization of activated carbon from rubber-seed shell by physical activation with steam, Biomass Bioenergy, 34 (2010) 539–544.
[29] IUPAC, Manual of symbols and terminology for physico-chemical quantities and units, appendix II, part I, definitions, terminology symbols in colloid and surface chemistry, Pure Appl. Chem., 31 (1972) 583–586.
[30] S. Shakoor, A. Nasar, Removal of methylene blue dye from artificially contaminated water using citrus limetta peel waste as a very low cost adsorbent, J. Taiwan Inst. Chem. Eng., 66 (2016) 154–163.
[31] A.E. Pirbazari, E. Saberikhah, M. Badrouh, M.S. Emami, Alkali treated foumanat tea waste as an efficient adsorbent for methylene blue adsorption from aqueous solution, Water Resour. Ind., 6 (2014) 64–80.
[32] O.S. Bello, Adsorptive removal of malachite green with activated carbon prepared from oil palm fruit fibre by KOH activation and CO_2 gasification, S. Afr. J. Chem., 66 (2013) 32–41.
[33] N. Mohammadi, H. Khani, V.K. Gupta, E. Amereh, S. Agarwal, Adsorption process of methyl orange dye onto mesoporous carbon material–kinetic and thermodynamic studies, J. Colloid Interface Sci., 362 (2011) 457–462.
[34] I. Langmuir, The constitution and fundamental properties of solids and liquids. Part I. Solids, J. Am. Chem. Soc., 38 (1916) 2221–2295.
[35] T.W. Weber, R.K. Chakravorti, Pore and solid diffusion models for fixed-bed adsorbers, AIChE J., 20 (1974) 228–238.
[36] A.A. Oladipo, M. Gazi, S. Saber-Samandari, Adsorption of anthraquinone dye onto eco-friendly semi-IPN biocomposite hydrogel: equilibrium isotherms, kinetic studies and optimization, J. Taiwan Inst. Chem. Eng., 45 (2014) 653–664.
[37] B.H. Hameed, D.K. Mahmoud, A.L. Ahmad, Equilibrium modeling and kinetic studies on the adsorption of basic dye by a low-cost adsorbent: coconut (*Cocos nucifera*) bunchwaste, J. Hazard. Mater., 158 (2008) 65–72.
[38] B.H. Hameed, A.T. Mohd Din, A.L. Ahmad, Adsorption of methylene blue onto bamboo-based activated carbon: kinetics and equilibrium studies, J. Hazard. Mater., 141 (2007) 819–825.
[39] N. Kannan, M.M. Sundaram, Kinetics and mechanism of removal of methylene blue by adsorption on various carbons-a comparative study, Dyes Pigm., 51 (2001) 25–40.
[40] T.A. Saleh, M.N. Siddiqui, A.A. Al-Arfaj, Kinetic and intraparticle diffusion studies of carbon nanotubes-titania for desulfurization of fuels, Pet. Sci. Technol., 34 (2016) 1468–1474.
[41] Y.S. Ho, G. McKay, Pseudo-second order model for sorption processes, Process Biochem., 34 (1999) 451–465.
[42] Q. Zhu, G.D. Moggridge, C. D'Agostino, Adsorption of pyridine from aqueous solutions by polymeric adsorbents MN 200 and MN 500. Part 2: kinetics and diffusion analysis, Chem. Eng. J., 306 (2016) 1223–1233.
[43] V.J.P. Poots, G. McKay, J.J. Healy, The removal of acid dye from effluent using natural adsorbents-I peat, Water Res., 10 (1976) 1061–1066.
[44] M. Doğan, H. Abak, M. Alkan, Adsorption of methylene blue onto hazelnut shell: Kinetics, mechanism and activation parameters, J. Hazard. Mater., 164 (2009) 172–181.
[45] Z. Shahryari, A.S. Goharrizi, M. Azadi, Experimental study of methylene blue adsorption from aqueous solutions onto carbon nanotubes, Int. J. Water Resour. Environ. Eng., 2 (2010) 016–028.
[46] K.G. Bhattacharyya, A. Sharma, Kinetics and thermodynamics of methylene blue adsorption on neem (*Azadirachta indica*) leaf powder, Dyes Pigm., 65 (2005) 51–59.
[47] W.H. Cheung, Y.S. Szeto, G. McKay, Intraparticle diffusion processes during acid dye adsorption onto chitosan, Bioresour. Technol., 98 (2007) 2897–2904.
[48] L. Liu, S. Fan, Y. Li, Removal behavior of methylene blue from aqueous solution by tea waste: kinetics, isotherms and mechanism, Int. J. Environ. Res. Public Health, 15 (2018) 1321, doi: 10.3390/ijerph15071321.